Aberrant intracellular metabolism of T-DM1 confers T-DM1 resistance in human epidermal growth factor receptor 2-positive gastric cancer cells

Hongbin Wang,[1,2] Wenqian Wang,[1] Yongping Xu,[1] Yong Yang,[1] Xiaoyan Chen,[1] Haitian Quan[1] and Liguang Lou[1] (iD)

[1]Shanghai Institute of Materia Medica, Chinese Academy of Sciences, Shanghai; [2]University of Chinese Academy of Sciences, Beijing, China

Trastuzumab emtansine (T-DM1), an antibody–drug conjugate (ADC) consisting of human epidermal growth factor receptor 2 (HER2)-targeted mAb trastuzumab linked to antimicrotubule agent mertansine (DM1), has been approved for the treatment of HER2-positive metastatic breast cancer. Acquired resistance has been a major obstacle to T-DM1 treatment, and mechanisms remain incompletely understood. In the present study, we established a T-DM1-resistant N87-KR cell line from HER2-positive N87 gastric cancer cells to investigate mechanisms of acquired resistance and develop strategies for overcoming it. Although the kinetics of binding, internalization, and externalization of T-DM1 were the same in N87-KR cells and N87 cells, N87-KR was strongly resistant to T-DM1, but remained sensitive to both trastuzumab and DM1. T-DM1 failed to inhibit microtubule polymerization in N87-KR cells. Consistently, lysine-MCC-DM1, the active T-DM1 metabolite that inhibits microtubule polymerization, accumulated much less in N87-KR cells than in N87 cells. Furthermore, lysosome acidification, achieved by vacuolar H$^+$-ATPase (V-ATPase), was much diminished in N87-KR cells. Notably, treatment of sensitive N87 cells with the V-ATPase selective inhibitor bafilomycin A1 induced T-DM1 resistance, suggesting that aberrant V-ATPase activity decreases T-DM1 metabolism, leading to T-DM1 resistance in N87-KR cells. Interestingly, HER2-targeted ADCs containing a protease-cleavable linker, such as hertuzumab-vc-monomethyl auristatin E, were capable of efficiently overcoming this resistance. Our results show for the first time that a decrease in T-DM1 metabolites induced by aberrant V-ATPase activity contributes to T-DM1 resistance, which could be overcome by HER2-targeted ADCs containing different linkers, including a protease-cleavable linker. Accordingly, we propose that V-ATPase activity in lysosomes is a novel biomarker for predicting T-DM1 resistance.

Gastric cancer is one of the most frequent human malignancies and the second-leading cause of cancer-related deaths worldwide.[1] There is mounting evidence that HER2 (ErbB2) overexpression is important in patients with gastric and gastroesophageal junction cancer.[2–4] Trastuzumab, a humanized mAb against HER2, has been approved, in combination with chemotherapy, as a new standard option for patients with HER2-positive advanced gastric or gastroesophageal cancer.[5]

Trastuzumab emtansine (T-DM1), an ADC comprising the HER2-targeted antibody trastuzumab and the antimicrotubule agent mertansine (DM1, a derivative of maytansine) containing a non-cleavable linker was approved by the FDA in February 2013 to treat HER2-positive metastatic breast cancers.[6] Binding of T-DM1 to HER2 triggers internalization of the HER2–T-DM1 complex into the cell through receptor-mediated endocytosis.[7,8] The DM1-containing metabolite, lysine-MCC-DM1, which is produced through lysosome-dependent proteolytic degradation of T-DM1, plays a major role in the tumor activity of T-DM1 through inhibition of microtubule assembly, which ultimately causes cell death.[9,10] Because the non-cleavable linker is stable in both the circulation and the tumor microenvironment, release of active DM1 occurs only as a result of lysosome degradation in cells, a property ensured by the activity of V-ATPase, which achieves a highly acidic pH (≤5) that promotes optimal activity of various hydrolases and vesicular transport.[11] Despite favorable initial outcomes, most HER2-positive patients treated with T-DM1 remain incurable because of the ultimate development of acquired resistance.[12–14] In addition, some HER2-positive cancers are primarily non-responsive or are only minimally responsive to T-DM1.[15] Thus, understanding resistance mechanisms and exploring strategies for overcoming T-DM1 resistance are urgent priorities.

In the present study, we used HER2-positive N87 gastric cancer cells to establish a T-DM1-resistant cell line termed N87-KR. We found that aberrant activity of V-ATPase in lysosomes of N87-KR cells results in defects in T-DM1 metabolism and thus a decrease in the T-DM1 metabolite, leading to

failure to inhibit microtubule polymerization and, ultimately, T-DM1 resistance. Moreover, H-MMAE, another HER2-targeted ADC containing a cleavable linker, was able to overcome T-DM1 resistance in N87-KR cells. Thus, we propose that V-ATPase activity in lysosomes may be a novel biomarker for predicting T-DM1 resistance, and further suggest that ADCs with cleavable linkers may be used to overcome T-DM1 resistance in patients with decreased tumor lysosome V-ATPase activity.

Materials and Methods

Reagents and antibodies. Both T-DM1 and trastuzumab were purchased from F. Hoffmann-La Roche (Basel, Switzerland). DM1 was provided by Jiangsu Hengrui Pharmaceutical Co. (Lianyungang, China). Bafilomycin A1 was obtained from Selleck Chemicals (Houston, TX, USA). DyLight 488 NHS Ester and LysoTracker Deep Red were purchased from Thermo Fisher Scientific (Waltham, MA, USA). Propidium iodide, sulforhodamine B, and DAPI were purchased from Sigma-Aldrich (St. Louis, MO, USA). Acridine orange was purchased from China National Pharmaceutical Industry Corp (Beijing, China). Hertuzumab-vc-MMAE was obtained from Rongchang Pharmaceuticals, Ltd (Yantai, China).

Antibodies against HER2, GAPDH, and PARP were purchased from Cell Signaling Technology (Beverly, MA, USA). The antibody specific for β-tubulin was purchased from Sigma-Aldrich. The antibody against β-actin was purchased from Santa Cruz Biotechnology (Santa Cruz, CA, USA). Alexa Fluor 488-conjugated goat anti-mouse IgG was purchased from Invitrogen (Carlsbad, CA, USA).

Cell culture and treatment. The N87 cell line was obtained from ATCC (Manassas, VA, USA). Cells were cultured according to the instructions provided by ATCC, and were tested and authenticated by Genesky Biotechnologies (Shanghai, China).

N87-KR cells were established by chronic exposure of N87 cells to gradually increasing concentrations of T-DM1 from initial 50 ng/mL to ultimate 1 μg/mL. After 18 months, the resistant cells were selected as polyclonal T-DM1-resistant N87KR cells and T-DM1-resistant monoclones were selected through the limiting dilution method.

Cell proliferation assay. Cell proliferation was determined by sulforhodamine B assay, as described previously.[16,17] In brief, cells seeded in 96-well plates were incubated for approximately 24 h and then treated with different concentrations of drugs for 72 or 120 h in culture medium containing 10% FBS.

Western blot analysis. Western blotting was carried out as described previously.[16] In brief, cells were lysed in SDS sample buffer, then separated by SDS-PAGE, and transferred to PVDF membranes (Millipore, Bedford, MA, USA). Membranes were incubated with primary antibodies at 4°C overnight and then with secondary antibodies for 2 h at room temperature. Immunoreactive proteins were detected using the Western blot image system from Thermo Fisher Scientific.

Cell cycle analysis. Cells were collected and fixed in ice-cold 70% ethanol overnight at −20°C. After staining with propidium iodide, the DNA content of cells was measured using a FACScan flow cytometer (BD Biosciences, San Jose, CA, USA) and analyzed with FlowJo 7.6 software.

Polymeric tubulin fraction assay. After drug treatment, cells were lysed and extracted for 3 min at room temperature with buffer consisting of 80 mM MES-KOH (pH 6.8), 1 mM MgC1$_2$, 1 mM EGTA, 0.1% Triton X-100, 10% glycerol, and protease inhibitors. The detergent-insoluble fraction containing cytoskeletal polymerized microtubules was analyzed by Western blotting.[18]

Binding, endocytosis, and recycling assays using cell-surface fluorescence quenching. *Binding assay.* Cells on 6-well plates were surface-labeled by incubating on ice for 1 h with DyLight 488 NHS Ester-linked T-DM1 (1 mg/mL). After washing three times with cold FACs buffer (2% FBS/PBS), cells were incubated on ice for 15 min with trypsin, treated with an equal volume of FBS, sedimented at 1000 *g*, and analyzed for binding affinity by flow cytometry.

Endocytosis assay. After pre-binding T-DM1 by incubating on ice for 1 h, cells on 6-well plates were incubated in growth medium at 37°C for the indicated intervals to allow internalization of surface fluorescence, after which cells were rapidly chilled, detached, and sedimented as previously described.[19] Cells were then incubated on ice for 15 min with stripping buffer (ddH$_2$O, 0.05 M glycine [MW 75.07] pH 2.45, and 0.1 M NaCl) to quench surface fluorescence, and then washed three times with FACS buffer. Internalized fluorescence was analyzed immediately by flow cytometry.

Exocytosis assay. After pre-incubation with T-DM1 on ice for 1 h to allow binding, as described for the endocytosis assay above, cells in 6-well plates were incubated at 37°C for 1 h, then rapidly chilled and surface-quenched by incubating with stripping buffer on ice for 15 min. After washing three times with FACS buffer, cells were warmed to 37°C for the indicated intervals, then rapidly chilled, detached, surface-quenched, and analyzed by flow cytometry.[19]

Fluorescence microscopy. Cells were seeded overnight on 6-well plates (5 × 10^5 cells/well) containing a cover glass. Labeled T-DM1 was added, and the cells were incubated at 37°C for 24 h, with the lysosome fluorescent probe Lyso-Tracker Red (50 nM) added 1 h prior to observation. The culture medium was then removed, and cells were fixed with 4% paraformaldehyde for 15 min. For immunocytochemical detection of microtubule polymerization, cells were first fixed with 4% paraformaldehyde, and then permeabilized with 0.1% Triton X-100 for 5 min. Thereafter, cells were incubated first with anti-tubulin antibody (diluted 1:200 in 2% BSA/PBS) at 37°C for 2 h, and then with Alexa Fluor 488-conjugated goat anti-mouse IgG (diluted 1:200 in 2% BSA/PBS) for 1 h at 37°C. The nuclear compartment was stained with DAPI by incubating on ice for 30 min. All subsequent wash steps were carried out using PBS. Cells were imaged with a 60 × oil-immersion objective using an Olympus FV1000 confocal microscope (Tokyo, Japan).

Lysine-MCC-DM1 metabolite analysis. N87 and N87-16-8 cells were cultured in 6-well plates, treated with 10 μg/mL T-DM1 alone or with 10 μg/mL T-DM1 plus 1 nM Baf-A1, and incubated for the indicated time or 24 h. Cells were collected, washed three times with PBS, and then centrifuged at 1000 *g* for 10 min. The identities and concentrations of T-DM1 metabolites in precipitated cells were determined by HPLC/MS. Cells were disrupted and extracted by adding acetonitrile, and then ultrasonicated. Cell fragments were removed by centrifugation, and proteins in the supernatant were precipitated by adding 25 μL internal standard (IS) solution (levonorgestrel, 200 ng/mL) and 200 μL methanol to a 50-μL aliquot of the supernatant. The mixture was mixed by vortexing for 1 min and then centrifuged for 1 min at 14 000 *g*. The upper layer was injected for LC-MS/MS analysis.

The LC-MS/MS detection was carried out using an LC30AD ultra-fast LC system (Shimadzu, Kyoto, Japan) coupled to a Triple Quad 5500 tandem mass spectrometer (Sciex, Foster City,

CA, USA) equipped with a TurboIon Spray source. Chromatographic separation was carried out on a Triart C18 column (50 × 2.1 mm i.d., 1.9 μm; YMC, Shimadzu Corp., kyoto, Japan). The mobile phase used for gradient elution consisted of 5 mM ammonium acetate : aqueous formic acid (100:0.2, v/v) and acetonitrile. Mass spectrometer detection was operated in the positive multiple reactions monitoring mode.

***In vivo* study.** Female nude mice (BALB/cA-nude, 5–6 weeks old) were purchased from Shanghai SLAC Laboratory Animal Co. (Shanghai, China). A tumor model was created by s.c. implanting 5×10^7 N87 or N87-16-8 cells into nude mice. Forty-eight hours after inoculation, mice were randomized into six groups and treated with vehicle (60% PEG-400), T-DM1 (10 mg/kg, i.v.), or H-MMAE (3 mg/kg, i.v.) once for a total of 21 days. Tumor volume was calculated as $width^2 \times length \times 0.5$, and body weight was monitored as an indicator of general health. For pharmacodynamic studies, tumor tissues were collected and prepared in RIPA buffer and analyzed by Western blotting. All animal experiments were carried out in accordance with guidelines of the Institutional Animal Care and Use Committee at the Shanghai Institute of Materia Medica, Chinese Academy of Sciences (Shanghai, China).

Data analysis. Data were analyzed with GraphPad Prism software (GraphPad Software, Inc., San Diego, USA). Non-linear regression analyses were carried out to generate dose–response curves and to calculate IC_{50} values. Means ± SD were calculated automatically using this software. A paired two-tailed Student's *t*-test was used to test for significance where indicated.

Results

Gastric N87-KR cells are selectively resistant to T-DM1. To investigate the molecular mechanism of T-DM1 resistance, we first established T-DM1-resistant clones of the N87 gastric cancer cell line. N87 cells were grown in medium containing gradually increasing concentrations of T-DM1, ultimately yielding 14 subclones of T-DM1-resistant N87 cells (N87-KR cells), as outlined in Table 1. These N87-KR cells were strongly resistant to T-DM1, with resistance ratios ranging from 47 to 104; however, they were sensitive to trastuzumab and DM1, with resistance ratios close to 1 (Table 1, Fig. 1a). N87-KR cells were also sensitive to other HER2-targeted agents, such as HKI-272 and lapatinib, as well as the microtubule-disrupting agent, vinorelbine, and the heat shock protein 90 inhibitor, geldanamycin (data not shown). As initial studies suggested that all of these N87-KR subclones showed the same mechanism of T-DM1 resistance, we focused mainly on N87-16-8 cells in the present study. Treatment with 1 μg/mL T-DM1 significantly increased G_2/M cell-cycle arrest and levels of cleaved PARP, an apoptosis biomarker, in N87 cells, as did DM1 (Fig. 1b,c). In contrast, DM1, but not T-DM1, induced G_2/M cell-cycle arrest and PARP cleavage at a concentration of 1 μg/mL in N87-16-8 cells (Fig. 1b,c). Taken together, these results indicate that N87-KR cells are selectively and strongly resistant to T-DM1.

T-DM1 binding, internalization, and externalization are not involved in T-DM1 resistance in N87-KR cells. T-DM1 exerts its antitumor activity through several critical steps, including binding to HER2, circulating with HER2 in cells (internalization and externalization), and proteolytic degradation into the active metabolite.[6] Factors that affect these steps may influence T-DM1 activity. We determined whether these steps had been altered in N87-KR cells. We first investigated the

Table 1. Antiproliferative effects of trastuzumab emtansine (T-DM1) and mertansine (DM1) against T-DM1-sensitive and -resistant cells

Cell line	IC_{50} (mean ± SD, nM)	
	T-DM1	DM1
N87	0.2 ± 0.1† (1)‡	2.3 ± 0.3 (1.0)§
N87-4-1	17.9 ± 0.2 (76)	4.9 ± 0.6 (2.1)
N87-4-2	20.4 ± 1.0 (86)	3.8 ± 0.3 (1.7)
N87-4-3	18.7 ± 13.4 (79)	2.8 ± 0.8 (1.2)
N87-4-4	21.9 ± 7.5 (92)	4.2 ± 0.9 (1.8)
N87-8-1	15.2 ± 0.1 (64)	2.3 ± 0.3 (1.0)
N87-8-3	20.8 ± 9.8 (88)	3.4 ± 0.7 (1.5)
N87-16-1	19.6 ± 9.6 (83)	2.7 ± 0.6 (1.2)
N87-16-2	13.8 ± 2.0 (58)	3.3 ± 0.5 (1.4)
N87-16-3	19.8 ± 9.0 (84)	3.4 ± 0.4 (1.5)
N87-16-4	13.1 ± 0.4 (56)	2.2 ± 0.5 (1.0)
N87-16-5	19.9 ± 9.1 (83)	3.1 ± 0.0 (1.3)
N87-16-6	24.7 ± 0.3 (104)	2.7 ± 0.5 (1.2)
N87-16-7	11.1 ± 2.6 (47)	3.5 ± 0.3 (1.5)
N87-16-8	12.5 ± 0.8 (53)	2.9 ± 1.3 (1.3)

†N87 and N87-KR cells were treated with different concentrations of T-DM1 for 120 h. ‡Resistance ratio = $IC_{50(N87-KR)}/IC_{50(N87)}$. §N87 and N87-KR cells were treated with different concentrations of DM1 for 72 h.

expression of HER2, which is essential for T-DM1 binding, in N87-16-8 cells. As shown in Figure 2(a), N87-16-8 cells expressed the same amount of HER2 as N87 cells. Consistent with this, both FACS analyses and confocal immunofluorescence assays indicated that T-DM1 bound to N87-16-8 cells and N87 cells with an equal maximum binding rate (Fig. 2b).

Next, the circulation of the T-DM1–HER2 complex was investigated in both N87-16-8 and N87 cells. As shown in Figure 2(c), internalization of T-DM1–HER2 complexes was initially detected within 30 min and reached a plateau after 1 h, achieving the same maximum internalization rates in both N87-16-8 and N87 cells. If T-DM1 externalization was investigated after internalization for 1 h, we found that the recycling curves for T-DM1 in both cell lines were similar and biphasic, with initial rapid recycling followed by a platform phase after 10 min (Fig. 2d). Collectively, these results indicate that binding, internalization, and externalization of T-DM1 are not involved in T-DM1 resistance.

Levels of the T-DM1 metabolite, lysine-MCC-DM1, are decreased in N87-KR cells. T-DM1, but not trastuzumab, causes G_2/M-phase cell-cycle arrest, apoptosis, and cell death through microtubule disruption.[20] As shown in Figure 3(a), 1 μg/mL T-DM1 or 6 nM DM1 significantly decreased polymerization of tubulin in N87 cells; however, only DM1, and not T-DM1, inhibited microtubule polymerization in N87-16-8 cells. Similar results were obtained in confocal immunofluorescence assays, which showed that polymeric microtubules were intact after T-DM1 treatment for 24 h in N87-16-8 cells (Fig. 3b). Thus, these results indicate that T-DM1 fails to inhibit microtubule polymerization in N87-16-8 cells, which is likely the reason for T-DM1 resistance.

Given that T-DM1 inhibition of microtubule polymerization both *in vitro* and *in vivo* is mediated by lysine-MCC-DM1,[21,22] we next investigated the accumulation of lysine-MCC-DM1 in both N87-16-8 and N87 cells. Both cell lines were treated with 10 μg/mL T-DM1 for 3, 9, or 24 h, then the amount of lysine-MCC-DM1 in cells was analyzed by
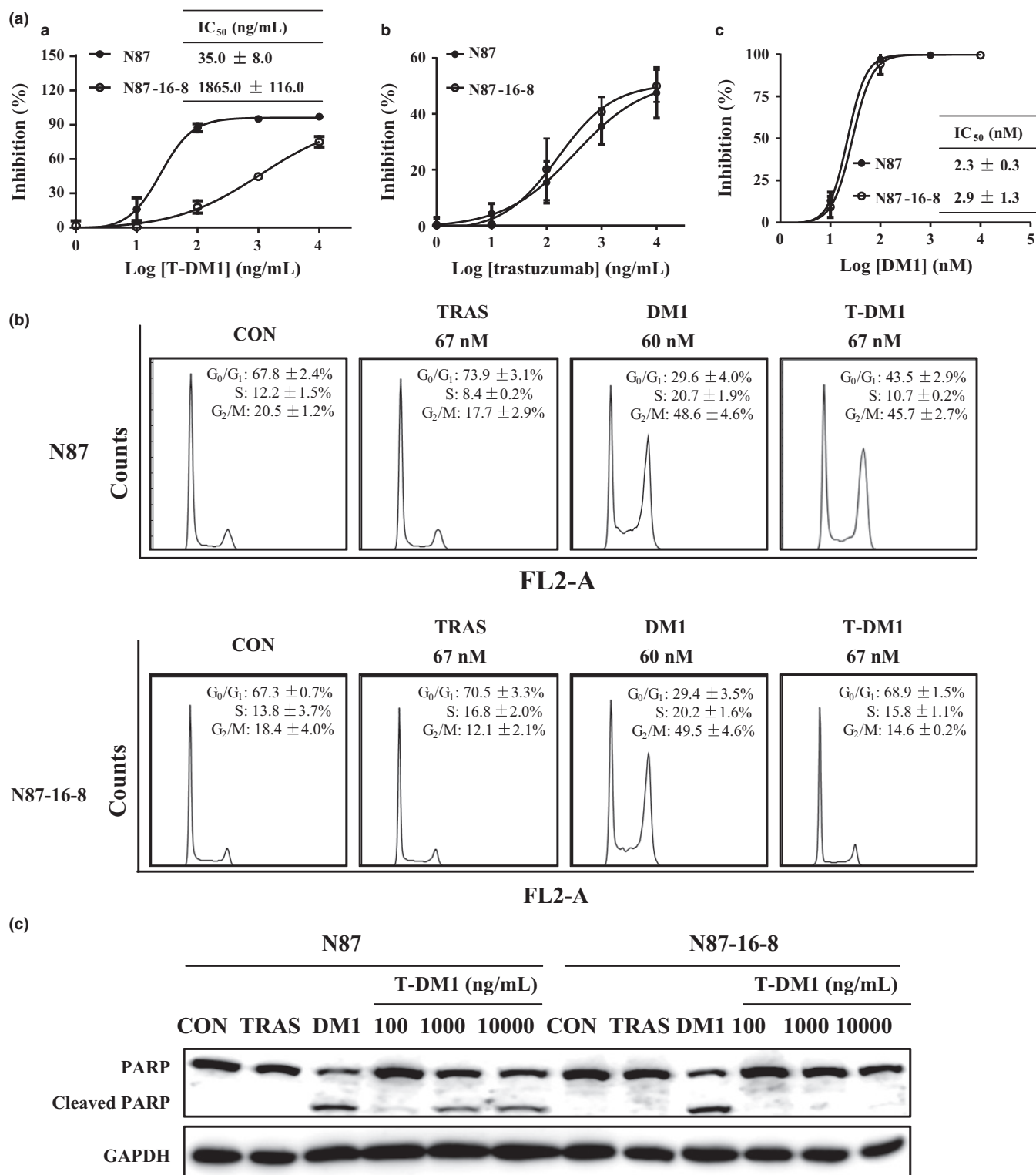
Fig. 1. N87-16-8 cells are resistant to trastuzumab emtansine (T-DM1), but remain sensitive to trastuzumab and mertansine (DM1). (a) Parental N87 cells and N87-16-8 cells were treated with the indicated concentrations of T-DM1 (a) or trastuzumab (b) for 120 h, or with DM1 (c) for 72 h. Cell survival was analyzed by sulforhodamine B assay. (b) N87 and N87-16-8 cells were treated with 10 μg/mL trastuzumab (TRAS), 60 nM DM1, or 1 μg/mL T-DM1 for 24 h. The cell cycle was analyzed by flow cytometry. Data are presented as means ± SD of three independent experiments. (c) N87 and N87-16-8 cells were treated with 10 μg/mL trastuzumab, 60 nM DM1, or the indicated concentrations of T-DM1 for 48 h, then were lysed for Western blot analysis of cleaved poly-(ADP-ribose) polymerase (PARP). The concentration of 10 μg/mL T-DM1 is 67 nM. CON, control.

HPLC-MS. Lysine-MCC-DM1 accumulated in a time-dependent manner in both N87 and N87-16-8 cells; however, the amount of lysine-MCC-DM1 in N87 cells was approximately 1.8-fold greater than that in N87-16-8 cells after exposure to T-DM1 for 24 h (Fig. 3c). Thus, these results collectively suggest that decreases in lysine-MCC-DM1 levels are responsible
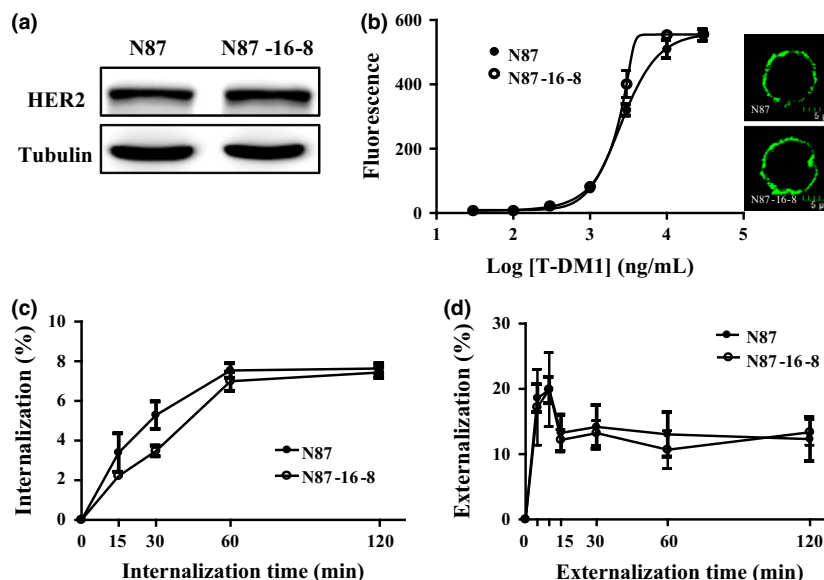
Fig. 2. Binding, internalization, and externalization of trastuzumab emtansine (T-DM1) are not significantly different between N87 and N87-16-8 cells. (a) Human epidermal growth factor receptor 2 (HER2) expression in N87 and N87-16-8 cells was analyzed by Western blotting. (b) N87 and N87-16-8 cells were treated with 1 μg/mL DyLight 488 NHS Ester-labeled T-DM1 on ice for 1 h and washed three times with cold FACS buffer, after which binding of T-DM1 to cells was analyzed by flow cytometry. (c) N87 and N87-16-8 cells were treated with 1 μg/mL DyLight 488 NHS Ester-labeled T-DM1 on ice for 1 h, washed three times, then incubated at 37°C for the indicated times to allow T-DM1 internalization. T-DM1 internalization was then analyzed by flow cytometry. (d) After pretreatment with 1 μg/mL DyLight 488 NHS Ester-labeled T-DM1 on ice for 1 h, N87 and N87-16-8 cells were incubated at 37°C for 1 h, then surface-quenched, washed three times, and incubated at 37°C for 5 min, 10 min, and the indicated intervals to allow T-DM1 externalization. T-DM1 externalization was then analyzed by flow cytometry.

for the inability to inhibit microtubule polymerization, leading to T-DM1 resistance in N87-KR cells.

Aberrant V-ATPase activity contributes to the decrease in lysine-MCC-DM1 in N87-KR cells. As there were no differences in T-DM1 binding, internalization, or externalization between N87 and N87-16-8 cells, the decrease in lysine-MCC-DM1 in N87-16-8 cells is likely attributable to a change in the lysosome system, in which T-DM1 is proteolytic degraded to lysine-MCC-DM1. As a proton pump that uses energy from ATP hydrolysis to produce a proton gradient, V-ATPase has been reported to play a critical role in proteolytic degradation in lysosomes.[9,23] Thus, to determine whether V-ATPase status was related to T-DM1 resistance, we investigated the effect of V-ATPase on T-DM1 degradation. To assess this, we used the selective V-ATPase inhibitor, Baf-A1. Although N87 and N87-16-8 cells were equally sensitive to Baf-A1 alone (Fig. 4a), distinctly different results were obtained in cells treated with T-DM1 plus 1 nM Baf-A1. In N87-16-8 cells, Baf-A1 did not affect the IC_{50} value of T-DM1. In sharp contrast, Baf-A1 significantly decreased the potency of T-DM1 in N87 cells, increasing the IC_{50} value up to 63-fold (Fig. 4b), indicating that V-ATPase inhibition conferred T-DM1 resistance in N87 cells. In addition, Baf-A1 significantly antagonized T-DM1 effects on microtubule disruption and apoptosis in N87 cells (Fig. 4c,d). Bafilomycin A1 also induced a concentration-dependent decrease in lysine-MCC-DM1 production in N87 cells (Fig. 4e), suggesting that this inhibition of lysine-MCC-DM1 production is the mechanism underlying the antagonism of T-DM1 activity by Baf-A1.

The emission spectrum of acridine orange, used as a probe to assess acidification of organelles, shifts from green to red only when it accumulates at high concentrations in acidic compartments.[24] In N87 cells, red-orange fluorescence accumulated in discrete cytoplasmic organelles, a phenomenon that

was not seen in N87-16-8 cells, indicating a dramatic reduction in the acidification of N87-16-8 cells (Fig. 4f). Abundant internalized T-DM1 colocalized with markers of lysosomes after 24 h of treatment in N87 cells, whereas little colocalization of T-DM1 with lysosomes occurred in N87-16-8 cells (Fig. 4g). Moreover, Baf-A1 significantly antagonized organelle acidification as well as colocalization of the T-DM1–HER2 complex with lysosomes in N87 cells. In contrast, it barely affected these parameters in N87-16-8 cells (Fig. 4f,g), confirming that V-ATPase activity is much weaker in N87-16-8 cells than in N87 cells. Collectively, these results suggest that decreased lysosomal V-ATPase activity leads to a decrease in lysine-MCC-DM1 production, and that this decrease in lysine-MCC-DM1 confers T-DM1 resistance in N87-16-8 cells.

Resistance to T-DM1 is overcome by HER2 ADCs containing linkers different from that in T-DM1. Because a metabolic disorder is the key mechanism underlying T-DM1 resistance in N87-16-8 cells, we considered using another HER2-targeted ADC containing a distinct linker as an approach to overcoming T-DM1 resistance. Accordingly, we tested H-MMAE, consisting of the HER2-targeted antibody hertuzumab and the microtubule-disrupting drug MMAE joined by an enzyme-cleavable linker,[25] against T-DM1-resistant N87-16-8 cells. Hertuzumab-vc-MMAE exerted potent inhibitory effects on the proliferation of both N87 and N87-16-8 cells, showing equivalent IC_{50} values (Fig. 5a). Consistent with this, H-MMAE significantly inhibited microtubule polymerization and apoptosis in N87-16-8 cells (Fig. 5b,c), suggesting that H-MMAE efficiently overcomes T-DM1 resistance *in vitro*.

Finally, the activities of H-MMAE and T-DM1 against N87-16-8 cells were investigated *in vivo*. As shown in Figure 5(d), T-DM1 at a dose of 10 mg/kg inhibited the growth of N87 xenografts by 117.5%, but only inhibited N87-16-8 xenografts by 31.4%, suggesting that N87-16-8 cells are also resistant to

(a)

(b)

(c)
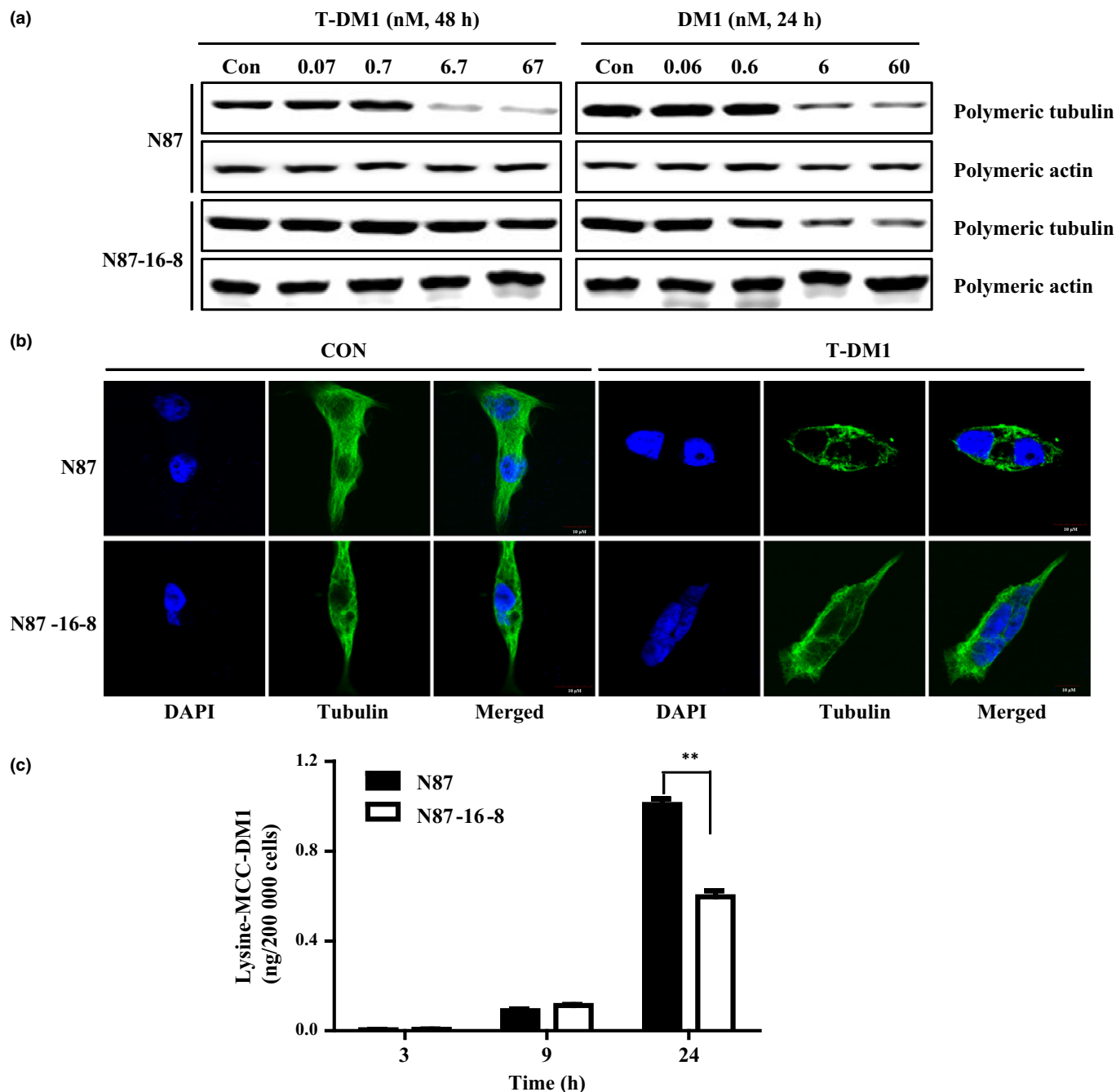
Fig. 3. Trastuzumab emtansine (T-DM1) fails to induce microtubule disassembly in N87-16-8 cells owing to decreased accumulation of lysine–MCC–mertansine (DM1). (a) N87 and N87-16-8 cells were treated with T-DM1 for 48 h or with DM1 for 24 h at the indicated concentrations. Cell lysates were extracted and polymeric tubulin was determined by Western blotting. Con, control. (b) After treatment with 1 μg/mL T-DM1 for 48 h, N87 and N87-16-8 cells were fixed, incubated with DAPI for 30 min, then incubated with an anti-tubulin primary antibody for 2 h, followed by incubation with Alexa Fluor 488-conjugated goat anti-mouse IgG. Cells were analyzed by confocal microscopy. Scale bar = 10 μm. CON, control. (c) N87 and N87-16-8 cells were treated with 10 μg/mL T-DM1 for the indicated times, after which the accumulation of lysine-MCC-DM1 was analyzed by HPLC–mass spectrometry. MCC: trans-4-(maleimidylmethylcyclohexane-1-carboxylate). Results are presented as means ± SD ($n = 3$; $^{**}P < 0.01$).

T-DM1 *in vivo*. This was confirmed by an investigation of the effects of T-DM1 on HER2 protein levels in tumor tissues, which showed that T-DM1 reduced HER2 expression only in N87 tumor tissues (Fig. 5f). These data were consistent with the *in vitro* results showing that T-DM1 only downregulated HER2 levels in N87 cells (data not shown). By contrast, H-MMAE at a dose of 3 mg/kg potently inhibited both N87 and N87-16-8 tumors, reducing their growth by 92.0% and 108.0%, respectively. Moreover, H-MMAE reduced the

expression of HER2 in both N87 and N87-16-8 tumor tissues (Fig. 5f). Taken together, these results indicate that H-MMAE efficiently overcomes T-DM1 resistance both *in vitro* and *in vivo*.

Discussion

Antibody–drug conjugates are emerging as a powerful class of antitumor agents.[26,27] However, drug resistance inevitably
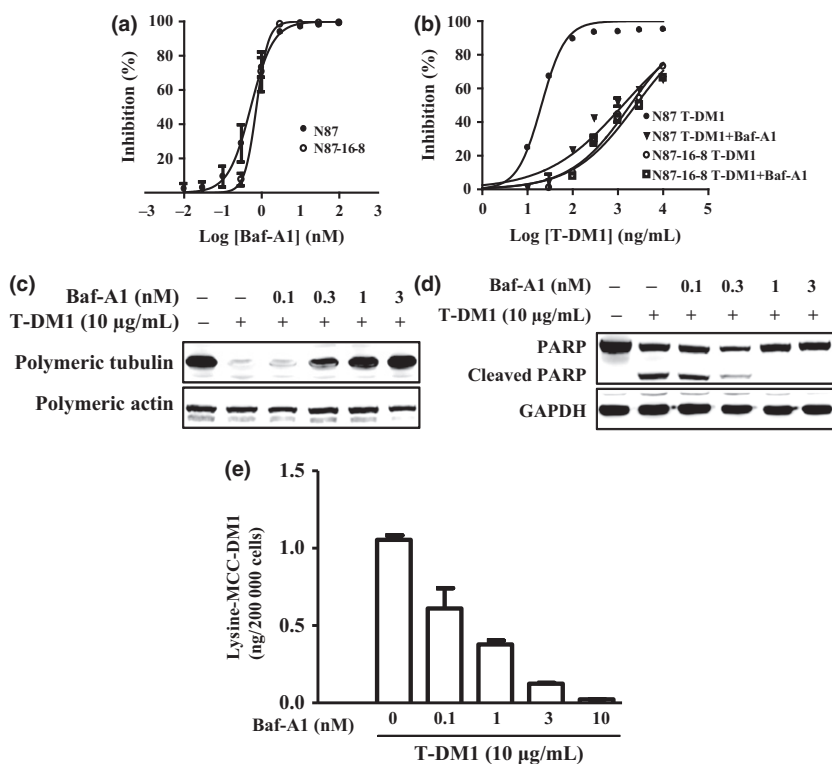
Fig. 4. Decrease in lysine–MCC–mertansine (DM1) levels in N87-16-8 cells may result from decreased vacuolar H$^+$-ATPase activity. (a) N87 and N87-16-8 cells were treated with different concentrations of bafilomycin A1 (Baf-A1) for 72 h, and cell proliferation was assessed using a sulforhodamine B assay. (b) N87 and N87-16-8 cells were treated with different concentrations of trastuzumab emtansine (T-DM1) alone or together with 1 nM Baf-A1 for 120 h, and cell proliferation was assessed using a sulforhodamine B assay. (c,d) Cells were treated with 10 μg/mL T-DM1 alone or together with different concentrations of Baf-A1 for 48 h, then polymeric tubulin, polymeric actin, poly-(ADP-ribose) polymerase (PARP), and GAPDH expression were determined by Western blot analysis using specific antibodies. (e) Lysine-MCC-DM1 levels were determined by HPLC/mass spectrometry after treatment with 10 μg/mL T-DM1 alone or together with the indicated concentrations of Baf-A1 for 24 h. (f) Cells were labeled with acridine orange for 30 min alone or together with 1 nM Baf-A1 for 24 h. (g) Confocal images of colocalization (yellow) of T-DM1–HER2 complexes with lysosomes in N87 and N87-16-8 cells. Cells were treated with 1 μg/mL DyLight 488 NHS Ester-labeled T-DM1 alone or together with 1 nM Baf-A1 for 24 h, then analyzed by confocal microscopy. MCC: trans-4-(maleimidylmethylcyclohexane-1-carboxylate). Scale bar = 5 μm.

develops following long-term treatment. Preclinical models can provide valuable tools for predicting likely mechanisms of resistance to these drugs, enabling drug-resistance mechanisms in the clinic to be identified, understood, and eventually overcome. We therefore modeled acquired resistance to T-DM1 using HER2-overexpressing gastric cancer N87 cells following chronic exposure to gradually increasing amounts of T-DM1. Few mechanisms of T-DM1 resistance have been reported. Here, we show for the first time that reducing the levels of the active T-DM1 metabolite, through decreased lysosomal V-ATPase activity, confers resistance to T-DM1. Notably, this resistance can be overcome by H-MMAE, another HER2-targeted ADC with an enzyme-cleavable linker.

Trastuzumab emtansine inhibits the growth of HER2-positive cancer cells through the actions of its two components: trastuzumab and DM1. Resistance to trastuzumab has been a major concern for years, and a number of possible mechanisms have been reported. These include increased epidermal growth factor receptor and HER3 expression,[28] reactivation of HER3 by transforming growth factor-β,[29] upregulation of insulin-like growth factor-1 receptor,[30] activation of SRC or c-Met,[31,32] a reduction in phosphatase and tensin homolog and constitutive activation of protein kinase B,[33,34] loss of p27^{Kip1} expression,[35–37] increased mucin 4 expression,[38,39] and activation of Notch signaling.[40] The main resistance mechanisms reported for microtubule disrupting agents include overexpression of P-glycoprotein,[41] or MDR-associated protein and breast cancer resistance protein,[42,43] mutation of tubulin,[44] and overexpression of βIII-tubulin.[45] Some resistance mechanisms for HER2-targeted ADCs have also been reported. Using in vitro T-DM1 resistance models from the HER2-overexpressing esophageal adenocarcinoma cell line OE-19, Sauveur and colleagues found that resistant cells became less sensitive to trastuzumab, and a subpopulation among the resistant cells showed increased expression of MDR1.[46] Loganzo

and colleagues reported that increased levels of the drug-efflux protein ABCC1 in 361-TM cells and decreased HER2 levels in JIMT1-TM cells were responsible for mediating resistance to trastuzumab–maytansinoid;[47] similar results were reported by Lewis Phillips.[48] It would appear to be self-evident that the resistance mechanisms of HER2-targeted ADCs primarily reflect resistance to the HER2-targeted antibody or the conjugated chemotherapeutic agent. In the current study, we revealed a novel resistance mechanism of HER2-targeted ADCs, showing that T-DM1 resistance in N87-KR cells is not contributed by trastuzumab or DM1, because N87-KR cells were sensitive to trastuzumab and DM1, as well as other HER2-targeted agents and microtubule-disrupting agents. Instead, T-DM1 resistance in N87-KR cells resulted from a T-DM1 metabolic disorder caused by reduced V-ATPase activity in lysosomes. Using an N87-TM cell drug-resistant model, Sung and colleagues reported findings that are congruent with our results. However, unlike our results, they reported that ADCs are internalized into caveolin 1-positive puncta, altering their trafficking to the lysosome and leading to T-DM1 resistance.[49] Interestingly, we also found that hertuzumab-vc-MMAE, another HER2-targeted ADC containing a cleavable linker, efficiently overcame T-DM1 resistance induced by metabolite reduction. Thus, the linker used in ADCs, which is typically neglected, should be accorded greater attention during the design of ADC structures.

Lysosomes provide a suitable pH and various proteolytic enzymes for the degradation of macromolecules, including some kinds of ADCs. Erickson and their coworkers have shown that lysosomal processing is required for the activity of antibody-maytansinoid conjugates, showing that Baf-A1, a selective V-ATPase inhibitor, almost completely abolished G$_2$/M cell-cycle arrest induced by huC242-SMCC-DM1.[9,50] It has also been reported that many drug-resistant cell lines have a lower intracellular pH than their drug-sensitive counterparts.

(f)

(g)
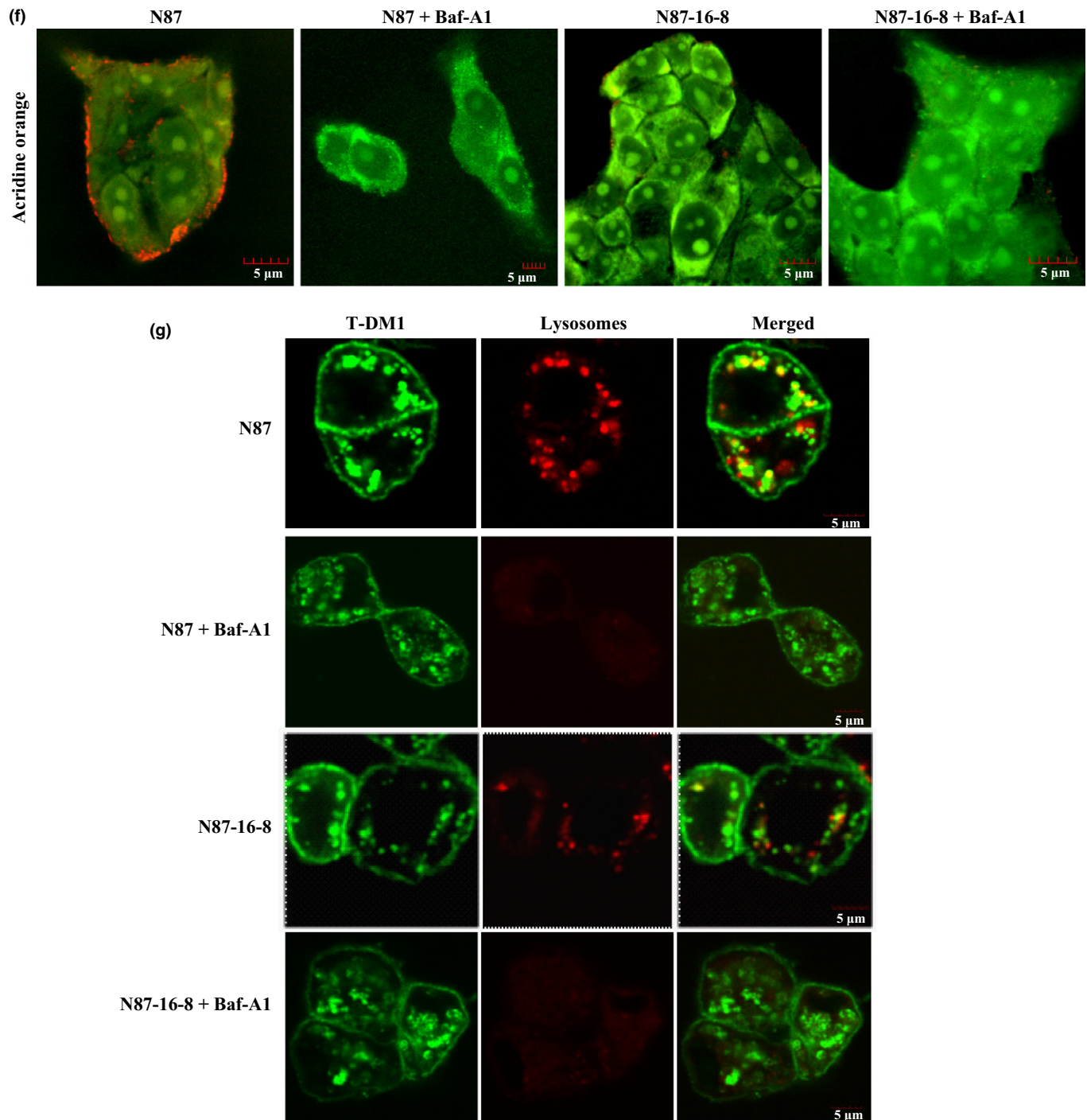
Fig. 4. Continued.

A decrease in cytotoxic effects owing to passive ion trapping-based lysosomal sequestration and an increase in the number of drug-accumulating lysosomes has been shown to enhance chemoresistance.[51] The data presented in the current study confirmed that a suitably acidified environment is essential for T-DM1 metabolism. Importantly, the N87-KR cell line established here showed dramatically reduced acidification. Thus, V-ATPase, which produces a proton gradient for proteolytic degradation of T-DM1, plays a critical role in the antitumor activity of T-DM1. A decrease in V-ATPase activity may inevitably disrupt T-DM1 metabolism and ultimately lead to

T-DM1 resistance, and the sole approach for overcoming this resistance is to find other drugs to replace T-DM1. Therefore, we propose that V-ATPase activity may serve as a biomarker for T-DM1 resistance. If a substantial reduction in V-ATPase activity is detected, T-DM1 is not suitable for use.

In conclusion, we reported a novel mechanism of T-DM1 resistance in which a decrease in the level of the active metabolite mediates T-DM1 resistance in HER2-positive gastric cancer cells. We propose that V-ATPase activity in lysosomes is a novel biomarker for predicting T-DM1 resistance and further suggest that HER2-targeted ADCs containing a

(a)

IC$_{50}$ (ng/mL)

N87	9.6 ± 0.2
N87 -16-8	9.2 ± 0.0

(b) N87   N87 -16-8

T-DM1(10 µg/mL)   − + −   − + −
H-MMAE (1 µg/mL)   − − +   − − +

PARP
Cleaved PARP
GAPDH

(c) N87   N87-16-8

T-DM1(10 µg/mL)   − + −   − + −
H-MMAE(1 µg/mL)   − − +   − − +

Polymeric tubulin
Polymeric actin

(d) N87

Vehicle
H-MMAE 3 mg/kg
T-DM1 10 mg/kg

****
****

(e) N87-16-8

Vehicle
H-MMAE 3 mg/kg
T-DM1 10 mg/kg

***

(f)   Control   T-DM1   H-MMAE

N87   HER2
Tubulin

N87-16-8   HER2
Tubulin
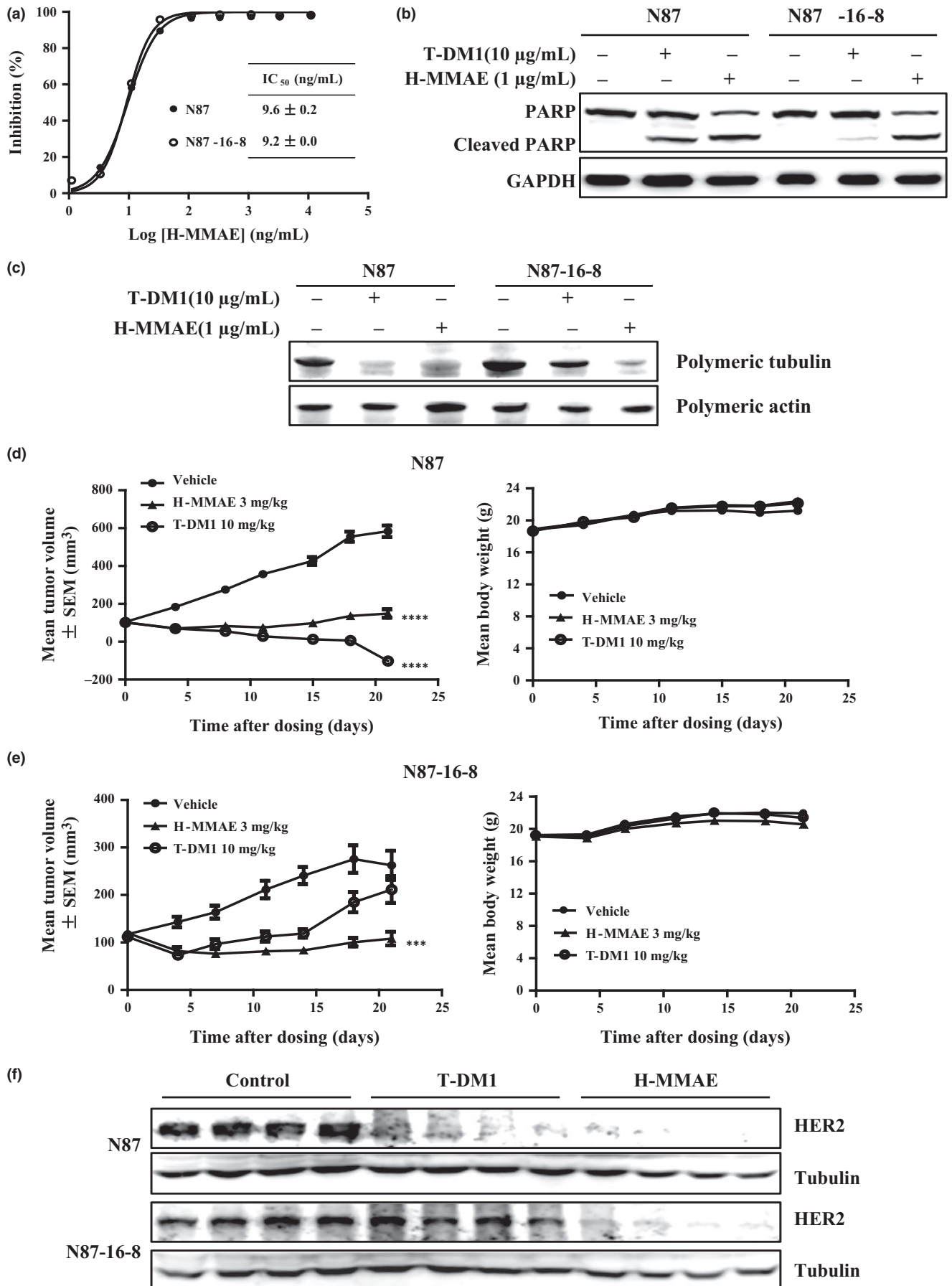
Fig. 5. Hertuzumab-vc-monomethyl auristatin E (H-MMAE) overcomes trastuzumab emtansine (T-DM1) resistance in N87-16-8 gastric cancer cells. (a) Growth inhibitory effects of H-MMAE on N87 and N87-16-8 cells following treatment for 120 h; IC_{50} values for H-MMAE are shown. (b,c) N87 and N87-16-8 cells were treated with 10 μg/mL T-DM1 or 1 μg/mL H-MMAE for 48 h, after which poly-(ADP-ribose) polymerase (PARP), polymeric tubulin, polymeric actin, and GAPDH expression were determined by Western blotting using specific antibodies. (d,e) Nude mice bearing N87 or N87-16-8 xenograft tumors were treated with vehicle, 10 mg/kg T-DM1, or 3 mg/kg H-MMAE weekly for 21 days. Tumor volume was measured on the indicated days. (f) Tumor tissues were lysed in RIPA buffer, and HER2 proteins levels were detected by Western blotting. (g) Photographs of reduced or disappeared tumors at the end of the experiment. Results are presented as means ± SEM (vehicle group, $n = 10$; treatment groups, $n = 8$). **$P < 0.01$; ***$P < 0.001$; ****$P < 0.0001$ *versus* respective control.
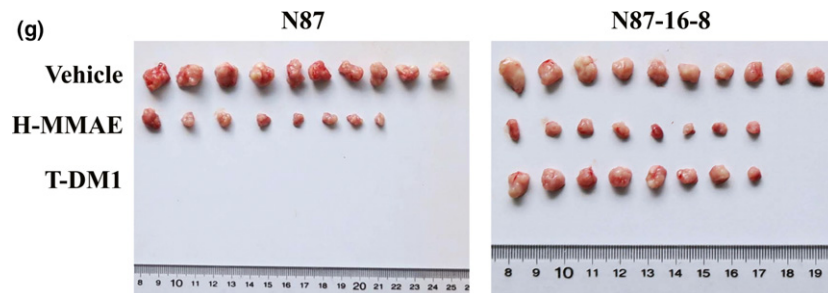
Fig. 5. Continued.

protease-cleavable linker are capable of overcoming T-DM1 resistance induced by the reduction in V-ATPase activity.

Acknowledgments

Disclosure Statement

The authors have no conflict of interests.

Abbreviations

ADC	antibody–drug conjugate
Baf-A1	bafilomycin A1
DM1	mertansine
HER2	human epidermal growth factor receptor 2
H-MMAE	hertuzumab-vc-MMAE
MCC	trans-4-(maleimidylmethylcyclohexane-1-carboxylate)
MMAE	monomethyl auristatin E
MS	mass spectrometry
MS/MS	tandem mass spectrometry
PARP	poly-(ADP-ribose) polymerase
T-DM1	trastuzumab emtansine
V-ATPase	vacuolar H^+-ATPase

References

1 Parkin DM, Bray F, Ferlay J, Pisani P. Global cancer statistics, 2002. *Ca-Cancer J Clin* 2005; **55**: 74–108.
2 Van Cutsem E, Sagaert X, Topal B, Haustermans K, Prenen H. Gastric cancer. *The Lancet* 2016; **388**: 2654–64.
3 Szász AM, Lánczky A, Nagy Á *et al.* Cross-validation of survival associated biomarkers in gastric cancer using transcriptomic data of 1,065 patients. *Oncotarget.* 2016; **7**: 49322–33.
4 Hofmann M, Stoss O, Shi D *et al.* Assessment of a HER2 scoring system for gastric cancer: results from a validation study. *Histopathology* 2008; **52**: 797–805.
5 Bang Y-J, Van Cutsem E, Feyereislova A *et al.* Trastuzumab in combination with chemotherapy versus chemotherapy alone for treatment of HER2-positive advanced gastric or gastro-oesophageal junction cancer (ToGA): a phase 3, open-label, randomised controlled trial. *The Lancet* 2010; **376**: 687–97.
6 Barok M, Joensuu H, Isola J. Trastuzumab emtansine: mechanisms of action and drug resistance. *Breast Cancer Res* 2014; **16**: 209.
7 Nolting B. Linker technologies for antibody–drug conjugates. *Antibody-Drug Conjugates* 2013; **1045**: 71–100.
8 Lewis Phillips GD, Li G, Dugger DL *et al.* Targeting HER2-positive breast cancer with trastuzumab-DM1, an antibody-cytotoxic drug conjugate. *Cancer Res* 2008; **68**: 9280–90.
9 Erickson HK, Park PU, Widdison WC *et al.* Antibody-maytansinoid conjugates are activated in targeted cancer cells by lysosomal degradation and linker-dependent intracellular processing. *Cancer Res* 2006; **66**: 4426–33.

10 Polakis P. Antibody drug conjugates for cancer therapy. *Pharmacol Rev* 2016; **68**: 3–19.
11 Saftig P. *Lysosomes*. New York: Landes Bioscience/Eurekah. Springer Science + Business Media, 2005.
12 Verma S, Miles D, Gianni L *et al.* Trastuzumab emtansine for HER2-positive advanced breast cancer. *New Engl J Med* 2012; **367**: 1783–91.
13 Hurvitz SA, Dirix L, Kocsis J *et al.* Phase II randomized study of trastuzumab emtansine versus trastuzumab plus docetaxel in patients with human epidermal growth factor receptor 2–positive metastatic breast cancer. *J Clin Oncol* 2013; **31**: 2977.
14 Wildiers H, Kim S, Gonzalez-Martin A *et al.* T-DM1 for HER2-positive metastatic breast cancer (MBC): Primary results from TH3RESA, a phase 3 study of T-DM1 vs treatment of physician's choice. *Eur J Cancer* Elsevier Sci Ltd The Boulevard, Langford Lane, Kidlington, Oxford Ox5 1Gb, Oxon, England, 2013; S7–8.
15 Okines AF, Cunningham D. Trastuzumab in gastric cancer. *Eur J Cancer* 2010; **46**: 1949–59.
16 Wang W, Liu Y, Zhao Z *et al.* Y-632 inhibits heat shock protein 90 (Hsp90) function by disrupting the interaction between Hsp90 and Hsp70/Hsp90 organizing protein, and exerts antitumor activity in vitro and in vivo. *Cancer Sci* 2016; **107**: 782–90.
17 Wang Q, Quan H, Zhao J, Xie C, Wang L, Lou L. RON confers lapatinib resistance in HER2-positive breast cancer cells. *Cancer Lett* 2013; **340**: 43–50.
18 Quan H, Liu H, Li C, Lou L. 1,4-Diamino-2,3-dicyano-1,4-bis (methylthio) butadiene (U0126) Enhances the Cytotoxicity of Combretastatin A4 Independently of Mitogen-Activated Protein Kinase Kinase. *J Pharmacol Exp Ther* 2009; **330**: 326–33.

19 Austin CD, De Mazière AM, Pisacane PI *et al.* Endocytosis and sorting of ErbB2 and the site of action of cancer therapeutics trastuzumab and geldanamycin. *Mol Biol Cell* 2004; **15**: 5268–82.

20 Oroudjev E, Lopus M, Wilson L *et al.* Maytansinoid-antibody conjugates induce mitotic arrest by suppressing microtubule dynamic instability. *Mol Cancer Ther* 2010; **9**: 2700–13.

21 Erickson HK, Widdison WC, Mayo MF *et al.* Tumor delivery and in vivo processing of disulfide-linked and thioether-linked antibody-maytansinoid conjugates. *Bioconjugate Chem* 2010; **21**: 84–92.

22 Erickson HK, Lewis Phillips GD, Leipold DD *et al.* The effect of different linkers on target cell catabolism and pharmacokinetics/pharmacodynamics of trastuzumab maytansinoid conjugates. *Mol Cancer Ther* 2012; **11**: 1133–42.

23 Rock BM, Tometsko ME, Patel SK, Hamblett KJ, Fanslow WC, Rock DA. Intracellular catabolism of an antibody drug conjugate with a noncleavable linker. *Drug Metab Disps* 2015; **43**: 1341–4.

24 Zelenin A. Acridine orange as a probe for molecular and cell biology. *Fluorescent and Luminescent Probes for Biological Activity*. Academic Press, London, 1993, pp. 83–99.

25 Jiang J, Dong L, Wang L *et al.* HER2-targeted antibody drug conjugates for ovarian cancer therapy. *Eur J Pharm Sci* 2016; **93**: 274–86.

26 Lin K, Tibbitts J, Shen BQ. Pharmacokinetics and ADME characterizations of antibody-drug conjugates. *Methods Mol Biol* 2013; **1045**: 117–31.

27 Wakankar A, Chen Y, Gokarn Y, Jacobson FS. Analytical methods for physicochemical characterization of antibody drug conjugates. *MAbs-Austin* 2011; **3**: 161–72.

28 Narayan M, Wilken JA, Harris LN, Baron AT, Kimbler K, Maihle NJ. Trastuzumab-Induced HER reprogramming in "Resistant" breast carcinoma cells. *Cancer Res* 2009; **69**: 2191–4.

29 Xiao Z, Carrasco RA, Schifferli K *et al.* A potent HER3 monoclonal antibody that blocks both ligand-dependent and independent activities: differential impacts of PTEN status on tumor response. *Mol Cancer Ther* 2016; **15**: 689–701.

30 Wicki A, Mandalà M, Massi D *et al.* Acquired resistance to clinical cancer therapy: a twist in physiological signaling. *Physiol Rev* 2016; **96**: 805–29.

31 Zhang L, Zhang S, Yao J *et al.* Microenvironment-induced PTEN loss by exosomal microRNA primes brain metastasis outgrowth. *Nature* 2015; **527**: 100–4.

32 Miekus K. The Met tyrosine kinase receptor as a therapeutic target and a potential cancer stem cell factor responsible for therapy resistance (Review). *Oncol Rep* 2017; **37**: 647–56.

33 Ebbesen SH, Scaltriti M, Bialucha CU *et al.* Pten loss promotes MAPK pathway dependency in HER2/neu breast carcinomas. *P Natl Acad Sci* 2016; **113**: 3030–5.

34 Chan CTO, Metz MZ, Kane SE. Differential sensitivities of trastuzumab (Herceptin)-resistant human breast cancer cells to phosphoinositide-3 kinase (PI-3K) and epidermal growth factor receptor (EGFR) kinase inhibitors. *Breast Cancer Res Tr* 2005; **91**: 187–201.

35 Yakes FM, Chinratanalab W, Ritter CA, King W, Seelig SA, Arteaga CL. Herceptin-induced inhibition of phosphatidylinositol-3 kinase and Akt is required for antibody-mediated effects on p27, Cyclin D1, and antitumor action. *Cancer Res* 2002; **62**: 4132–41.

36 Le X, Claret F, Lammayot A *et al.* The role of cyclin-dependent kinase inhibitor p27Kip1 in anti-HER2 antibody-induced G1 cell cycle arrest and tumor growth inhibition. *J Biol Chem* 2003; **278**: 23441–50.

37 Nahta R, Takahashi T, Ueno NT, Hung M, Esteva FJ. P27kip1 down-regulation is associated with trastuzumab resistance in breast cancer cells. *Cancer Res* 2004; **64**: 3981–6.

38 Nagy P, Friedlander E, Tanner M *et al.* Decreased accessibility and lack of activation of ErbB2 in JIMT-1, a Herceptin-Resistant, MUC4-Expressing breast cancer cell line. *Cancer Res* 2005; **65**: 473–82.

39 Priceschiavi SA, Jepson S, Li P *et al.* Rat Muc4 (sialomucin complex) reduces binding of anti-ErbB2 antibodies to tumor cell surfaces, a potential mechanism for herceptin resistance. *Int J Cancer* 2002; **99**: 783–91.

40 Osipo C, Patel P, Rizzo P *et al.* ErbB-2 inhibition activates Notch-1 and sensitizes breast cancer cells to a gamma-secretase inhibitor. *Oncogene* 2008; **27**: 5019.

41 Yu S-F, Zheng B, Go M *et al.* A novel anti-CD22 anthracycline-based antibody–drug conjugate (ADC) that overcomes resistance to auristatin-based ADCs. *Clin Cancer Res* 2015; **21**: 3298–306.

42 Stavrovskaya AA, Stromskaya TP. Transport proteins of the ABC family and multidrug resistance of tumor cells. *Biochemistry-Us* 2008; **73**: 592–604.

43 Kovtun YV, Audette CA, Mayo MF *et al.* Antibody-maytansinoid conjugates designed to bypass multidrug resistance. *Cancer Res* 2010; **70**: 2528–37.

44 Drukman S, Kavallaris M. Microtubule alterations and resistance to tubulin-binding agents (review). *Int J Oncol* 2002; **21**: 621–8.

45 Rai A, Kapoor S, Naaz A, Santra MK, Panda D. Enhanced stability of microtubules contributes in the development of colchicine resistance in MCF-7 cells. *Biochem Pharmacol* 2017; **132**: 38–47.

46 Sauveur J, Chettab A, Cleret A, Savina A, Dumontet C. Mechanisms of resistance to trastuzumab emtansine in gastric cancer. *Cancer Res* 2016; **76**: 309.

47 Loganzo F, Tan X, Sung M *et al.* Tumor cells chronically treated with a Trastuzumab–Maytansinoid Antibody-Drug conjugate develop varied resistance mechanisms but respond to alternate treatments. *Mol Cancer Ther* 2015; **14**: 952–63.

48 Lewis Phillips G. Mechanisms of acquired resistance to trastuzumab emtansine (T-DM1). Presented at: World ADC Summit 2011; San Francisco, CA: London, UK: HansonWade; 2011. Google Scholar

49 Sung MS, Tan X, Hosselet C *et al.* Caveolae-mediated endocytosis as a novel mechanism of resistance to T-DM1 ADC. *Cancer Res* 2016; **76**: 2113.

50 Doronina SO, Mendelsohn BA, Bovee TD *et al.* Enhanced activity of monomethylauristatin F through monoclonal antibody delivery: effects of linker technology on efficacy and toxicity. *Bioconjugate Chem* 2006; **17**: 114–24.

51 Zhitomirsky B, Assaraf YG. Lysosomes as mediators of drug resistance in cancer. *Drug Resist Update* 2016; **24**: 23–33.